NUMERICAL SYNTHESIS DESIGN OF COUPLED RESONATOR FILTERS

S. Wen and L. Zhu

School of Electric and Electronic Engineering
Nanyang Technological University
Singapore 639798, Singapore

Abstract—This paper proposes a methodology for numerically synthesizing element values of coupled resonator filters. These element values are compatible in retrieving coupling matrix of a cross-coupled quadruplet structure (also known as the folded structure). Differed from direct synthesis by matrix rotation, numerical solution has been adopted here to its equivalent coupling model. For varied specified return loss, numerical solutions of these element values have been derived and their accuracy is verified with their analytical counterparts to be extended for stringent design requirement. In addition, multiple sets of data are tabulated and categorized for efficient filter synthesis design under different specified pass-band return loss. In the end, an example quadruplet filter is designed, fabricated and measured for validation of the presented synthesis design methodology.

1. INTRODUCTION

Ever since 1970s, the synthesis design of coupled resonator circuits has been discussed by numerous research groups. A. E. Atia, et al., in [1] and [2] elaborated the synthesis of coupling matrix for general filter functions. Started from the factorization of the two-port filter admittance, the original coupling matrix is obtained from the eigen-matrix and transformation matrix using the standard Darlington procedure [3]. Since transformation matrix is derived from the Gram-Schmidt Orthonormalization of its first and last rows, all the eigen-values related to an eigen-matrix can be preserved in the resultant coupling matrix. Here the eigen-values of the filter response will be determined in terms of the factorization from the two-port filter admittance. Normally after the original coupling matrix is created,

---

Corresponding author: L. Zhu (ezhul@ntu.edu.sg).

reduction and annihilation of matrix elements is still needed to make the coupling matrix realizable. Cameron in [4] and [5] thus introduced the direct synthesis for the folded cross-coupled structure to directly synthesize the practical coupling matrix according to the specified filter response without necessity of similarity transformation.

Differed from the general synthesis of coupling matrix, Levy's synthesis design [6] is based primarily on constructing an equivalent quadruplet structure and solving its element circuit values, adopting both an approximation method and a much more accurate synthesis also based on standard Darlington procedure [3]. Furthermore, Hong used this quadruplet structure to implement selective band-pass filters on planar microwave structure [8, 9]. The exact analysis on the filter element values requires comparatively complicated procedure [3] and [6], while the approximate analysis causes unacceptable inaccuracy when the selectivity requirement is high [6] and [8]. For this reason, Hong tabulated a list of design table for highly selective filter with a pair of finite transmission zeros as detailed in [7] and [8]. However, practical design demonstrated that the results are accurate but they are only valid on a certain range of pass-band return loss, besides, the data extraction itself still requires the standard Darlington procedure [3].

In this work, we will introduce an alternative methodology to synthesize the element values of the canonical quadruplet structure [6]. This methodology no longer requires the standard Darlington procedure to extract elemental circuit values (or its corresponding coupling matrix), yet the accuracy is retained as comparing to the approximate analysis [6]. This methodology used network analysis on the equivalent coupling circuit to retrieve its transmission parameter. In order to obtain the element values for the required filter specification, a set of determinant equations is achieved with actual physical meaning and pass-band return loss can be further included as a synthesis parameter. After systematic description is made, a prototype filter is fabricated for verification in experiment.

2. FILTER NETWORK AND SYNTHESIS

The equivalent quadruplet [6] (or folded [4]) structure was introduced and analyzed as a basic cross-coupled resonator filter network. Differed from [4] and [6], in this work, we would like to develop an alternative methodology to express its transmission parameter using the network parameters.

2.1. Equivalent Circuit Network

Figure 1 depicts a generalized equivalent network of the well-known quadruplet filter using unit or normalized parameters, i.e., g_1, g_2, J, J_1 and J_2. Herein, g_1 and g_2 are symbolized as the two individual resonators and they represent their shunt reactance in their LC models at a single frequency. Plus, the four resonators are set to resonate at the same required frequency. This example filter is terminated at two external ports, i.e., Ports 1 and 2, with matched load impedance.
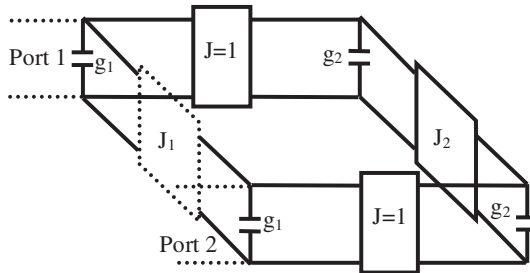

Figure 1. Equivalent network of cross-coupled quadruplet filter.

The parameters, J, J_1 and J_2, are symbolized as the immitance invertors which can be interpret by a set of coupled microstrip lines. The coupling coefficient between resonators is quantified by the normalized characteristic impendence of the immitance inverters. The middle-located inverter J is fixed at the unit '1'. Therefore, the tunable or undecided parameters are reactance g_1 and g_2, inverter J_1 and J_2. In addition, J_1 is dotted as a negative coupling quantity to be distinguished from J_2 and J. These two paths work together so as to realize a pair of finite transmission zeros in the lower and/or higher ranges than the desired pass-band. As this quadruplet network is established, the remaining problem is how to obtain the relationship between element values and specified filter response which is represented by those element values.

2.2. Network Parametric Description

Differed from the traditional synthesis methodology in a sense of coupling matrix, the element values are not directly obtained from transformation of its eigen matrix here. From the top part of Figure 1, a shunt structure can be formed and it consists of two branches in this quadruplet structure. On one hand, the longer branch (Path A) is formed by sequentially cascading the 1st resonator g_1, 1st mixed coupled inverter $J = 1$, 1st resonator g_2, the magnetically coupled

inverter J_2, 2nd resonator g_2, 2nd mixed coupled inverter $J = 1$ and 2nd resonator g_1. On the other hand, the shorter branch (Path B) only includes an electronically coupled inverter J_1. Therefore, these two branches or paths create a pair of routes so as to produce the expected cross coupling.

The overall transfer or ABCD matrix of the above longer branch can be simply derived as below by multiplying the transfer or ABCD matrices of every element matrix involved. The definition of these matrices is given in Table 1.

$$\begin{pmatrix} 1 & 0 \\ j \times s \times g_1 & 1 \end{pmatrix} \begin{pmatrix} 0 & j \\ j & 0 \end{pmatrix} \begin{pmatrix} 1 & 0 \\ j \times s \times g_2 & 1 \end{pmatrix} \begin{pmatrix} 0 & j/J_2 \\ j \times J_2 & 0 \end{pmatrix}$$

$$\cdot \begin{pmatrix} 1 & 0 \\ j \times s \times g_2 & 1 \end{pmatrix} \begin{pmatrix} 0 & j \\ j & 0 \end{pmatrix} \begin{pmatrix} 1 & 0 \\ j \times s \times g_1 & 1 \end{pmatrix} = \begin{pmatrix} T_{a11} & T_{a12} \\ T_{a21} & T_{a22} \end{pmatrix} \quad (1)$$

In Table 1, only the inverter matrices are frequency independent, so this can be helped to regulate the complexity of the synthesized transfer function and decide the degrees of its related polynomial function. In the following, the calculated transfer matrix will be used for numerically determining all four unknown element values, included in the transfer parameter expression based on the synthesis approach.

Similarly, the single-valued branch or Path B can be expressed as a unified transfer matrix as shown in Equation (2).

$$\begin{pmatrix} 0 & j/J_1 \\ j \times J_1 & 0 \end{pmatrix} = \begin{pmatrix} T_{b11} & T_{b12} \\ T_{b21} & T_{b22} \end{pmatrix} \quad (2)$$

Table 1. Definition of element matrices.

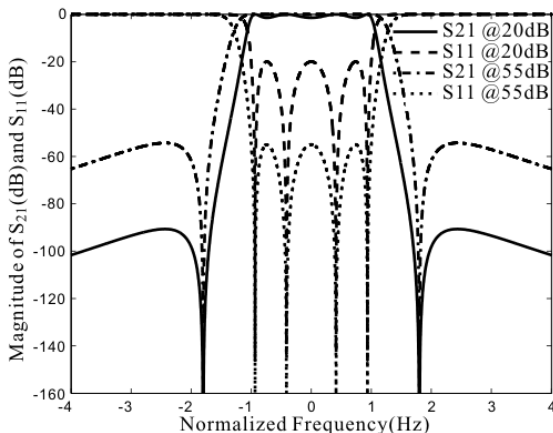| Element matrices	Corresponding circuit elements
$\begin{pmatrix} 1 & 0 \\ j \times s \times g_1 & 1 \end{pmatrix}$	Shunt reactance g_1
$\begin{pmatrix} 0 & j \\ j & 0 \end{pmatrix}$	Normalized inverter $J = 1$
$\begin{pmatrix} 1 & 0 \\ j \times s \times g_2 & 1 \end{pmatrix}$	Shunt reactance g_2
$\begin{pmatrix} 0 & j/J_2 \\ j \times J_2 & 0 \end{pmatrix}$	Inverter with characteristic admittance J_2
$\begin{pmatrix} T_{a11} & T_{a12} \\ T_{a21} & T_{a22} \end{pmatrix}$	Transfer matrix in Path A

Figure 2. Scattering parameters versus normalized frequency under the fixed locations of transmission poles and zeros.

Since the admittance parameter of every branch can be derived using the relationship between the admittance and transfer matrices as given in [10], the admittance matrix of the overall network in Figure 1 can be simply summed up by two parallel-connected branch admittance matrices, thereby getting its corresponding scattering matrix [10].

In this way, the transmission/reflection responses are expressed directly in terms of complex frequency variable s, with their polynomial coefficients described by element value g_1, g_2, J_1 and J_2.

2.3. Determined Solution

The element values are variables to be determined according to the specified filter response. Previously, pure matrix transformation has been used for exact synthesis of the element values or its correspondent coupling matrix. Differed from the standard Darlington Procedure in [1–6], the equation here is directly established from the transmission/reflection response instead of their eigenvalue and eigenvector expression. Taking the resultant forward transmission parameter S_{21} as an example below

$$S_{21} = \frac{n_2 s^2 + n_1 s + n_0}{d_4 s^4 + d_3 s^3 + d_2 s^2 + d_1 s + d_0} \tag{3}$$

Many coefficients in Equation (3) can be defined as below while

the coefficients undefined all have zero value.

$$n_2 = 2J_1g_2^2 \tag{4}$$

$$n_0 = 2(J_2 - J_1J_2^2) \tag{5}$$

$$d_4 = g_1^2g_2^2 \tag{6}$$

$$d_2 = -g_2^2 - g_2^2J_1^2 - 2g_1g_2 - g_1^2J_2^2 \tag{7}$$

$$d_1 = 2g_2 + 2g_1J_2^2 \tag{8}$$

$$d_0 = -2J_1J_2 + J_2^2 + J_1^2J_2^2 + 1 \tag{9}$$

Substituted by Equations (4)–(9), it can be well imaged that the forward transmission parameter becomes rather complicated as a rational function. For the evenly-equated filter function, we need six equations. Two are from numerator and four equations are from denominator of the rational function, respectively.

If we utilize the forward reflection parameter S_{11} for synthesis, an even complicated expression will be found. However, to solve the unknown element values, much less equations are required. For the unit quadruplet circuit as shown in Figure 1, only four equations are in fact required. Contrarily, over-determined equations may cause complexity in finding the solution, yet neither the accuracy nor the convergence will be enhanced.

Therefore, a set of determined equations here is required for standard solution on the quadruplet structure and its cascaded form. Since the polynomial expression on a continuous span of frequency spectrum would only result in the complicate rational expression, we try to find its discrete values with resorting to its frequency singularities. Below are the four determined equations.

$$\begin{cases} S_{11}(\text{reflection\_zero\_pair1}) = 0 \\ S_{11}(\text{reflection\_zero\_pair2}) = 0 \\ S_{21}(\text{transmission\_zero\_pair}) = 0 \\ S_{11}(\text{zero\_frequency}) = L_R \end{cases} \tag{10}$$

In Equation (10), the first two equations related to the reflection zero pair1 and pair2 create the four pass-band transmission poles and they can be found from the degree of denominator in the S_{21} or conversion of Equations (1) and (2). The third one is to determine a pair of transmission zero. Here we use the first three equations to quantitatively express the emergence of zero/poles. Finally, the last equation is achieved for the structures at zero frequency and it is used to indicate the specified return loss zero frequency. Therefore, the return loss at zero frequency can be specified as any expected level, which extends the design flexibility. As the scattering parameters

are derived in close form of frequency variable, four unknown element values can be solved in Equation (10) as the determined solutions of the equivalent circuit.

In our work herein, the determined equations are programmed in Matlab with the function solver to achieve controllable accuracy. The transmission zeros and poles are considered as the input condition in the numerical procedure. After element-values are solved, the coupling coefficient could directly be retrieved by the well-know formulas given in [6] or [8].

3. VERIFICATION AND TABULATED RESULT

In order to verify the synthesis results, we will at first directly derive the transmission and refection parameters of the filter network in Figure 1 under the available element values reported in [8]. Next, these element values are numerically solved with the determined synthesis solution described above to demonstrate the performances of the filter while is unable to be analyzed using the traditional synthesis design procedure.

3.1. Numerical Verification

First of all, the first row of element values was picked up from the design table 10.1 in [8] and used as the values of those elements in the filter network shown in Figure 1.

$$g_1 = 0.95974, \ g_2 = 1.42192, \ J_1 = -0.21083, \ J_2 = 1.11769 \qquad (11)$$

Since the coupling and resonating elements in Figure 1 have both been treated as ideal models, the solution of the polynomial equations in (10) will determine an ideal value of return loss. Corresponding to the case which has considered physical effects with the actual return loss of 20 dB in [8], the ideal return loss can be calculated as 46.053337 dB from Equation (3). With the known element values given in Equation (11), the transmission zeros can be found as ± 1.80000 while the transmission poles (or reflection zeros) at ± 0.412530 (or ± 0.935860). Thus the determined condition is fully constructed. The condition is achieved without correlation to the synthesis process in the unchanged circuit model shown in Figure 1. Under these above solutions, the element values in Figure 1 can be numerically determined as

$$g_1 = 0.959738, \ g_2 = 1.421912, \ J_1 = -0.210822, \ J_2 = 1.117680 \quad (12)$$

Look at the two sets of element values comparatively, we can figure out, numerical consistency between them has well been achieved with

the resultant synthesis accuracy at maximal six digits. Furthermore, the values listed in (12) hold a mathematical accuracy of seven digits. The verification can be quantitatively completed by specifying the return loss for the element value synthesis. The synthesis results are given in the first and last rows of Table 2. For the two different sets of element values with the fixed transmission zeros/plots but varied in-band return losses (i.e., 20 dB and 55 dB), the two sets of simulated frequency responses are plotted in Figure 2. So, the results given in Figure 2 demonstrate that the presented synthesis procedure can be executed to design a bandpass filter with differed pass/stop-band specification by setting up the varied return loss, thereby extending the flexibility in practical design.

Table 2. Element values of the quadruplet prototype in Figure 1.

Return loss (dB)	g_1	g_2	J_1	J_2
20	1.816298	1.202716	−0.191801	0.781716
25	1.554765	1.290542	−0.185933	0.864406
30	1.359285	1.350906	−0.185665	0.935367
35	1.206123	1.389664	−0.189626	0.997723
40	1.082111	1.411671	−0.197186	1.054084
45	0.979239	1.421151	−0.208100	1.106818
50	0.892293	1.421874	−0.222352	1.158216
55	0.817696	1.417274	−0.240083	1.210617

3.2. Tabulated Results

Table 2 provides a list of tabulated results from the ideal synthesis procedure under mathematical expression of transmission/reflection responses as in Equation (3). Here, transmission zero/poles are selected exactly the same as those described in chapter 3.1. This table can be used for direct reference on differed pass-band specification of high selective filter since the pole/zero locations are fixed in this table. As for varied transmission zero locations as shown in [8], the similar procedure in mathematics can be achieved to get a full set of design data, and therefore it is not detailed here.

4. FABRICATION AND MEASURED RESULTS

In addition to numerical simulation, the validation of the synthesis design is further preceded in this work by determining the entire

dimension of an actual filter circuit and fabricating such a filter on microstrip structure for experimental validation.   To do it, the commercial fullwave simulators can be utilized to establish the relationship between physical dimensions and electrical parameters as detailed in [7] and [9]. Now, let's take into account the coupling matrix of the filter network in Figure 1 as an example.   In this case, all altogether three types of coupling, i.e., electric, magnetic and hybrid coupling, need to be considered in the filter design.

Shown in Figure 3 is the layout for a typical magnetic coupling between two square ring resonators formed on the microstrip-line structure. In this case, the coupling coefficient is mainly dependent on the gap size of the square ring resonator. As the gap size is increased, the first resonant frequency of the coupled resonator is split to the two individual ones, and their distance becomes large.
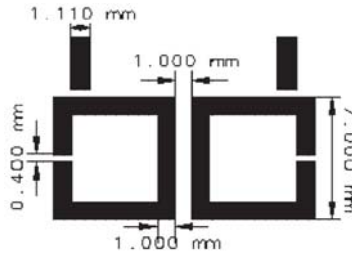

Figure 3.   Layout for numerical extraction of coupling coefficient between the two coupled resonators for varied coupling gap.
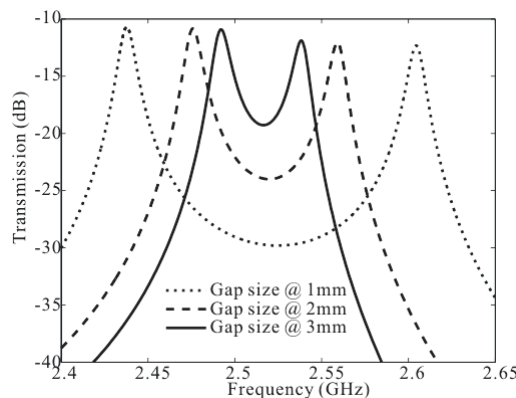

Figure 4.   Simulated frequency response for extracting coupling coefficient of two magnetically coupled resonators.

In this work, the initial resonant frequency is chosen in Agilent LineCalc[TM] as 2.5 GHz and the microstrip feed line is selected to have the characteristic impedance of 50 Ohm. Thereafter, actual dimensions can be decided by executing the fullwave simulation on its layout and they are marked in Figure 3. Now, let's study the coupling characteristics of magnetically coupled square ring resonators [9]. First, the two feed lines are loosely and capacitively coupled to the two individual resonators such that only the coupling between the resonators dominates the locations of the two split resonant frequencies [8].

Figure 4 shows the simulated transmission coefficient (S_{21}-magnitude) for three different gap sizes. As the gap size is reduced from 3 mm to 2 mm and 1 mm, the distance between the two resonant peaks are visibly moved far away with each other, thus indicating the enhanced coupling degree. The pass-/stop-band specification is synthesizable now directly by the element values, however, as
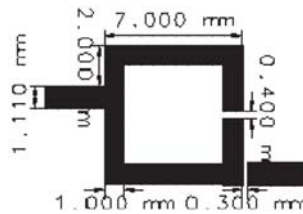

Figure 5. Layout for numerical extraction of external quality factor (tapping location @ 2 mm).
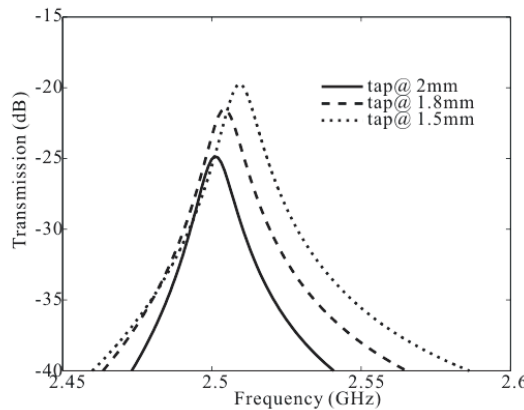

Figure 6. Simulated frequency responses for extracting quality factor.

an auxiliary tuning parameter, the same procedure can be used on the external quality factor to characterize its coupling degree by working out the correlation between the tap position and the resonator fractional bandwidth. Figure 5 is the physical layout for numerical extraction of the coupling degree while Figure 6 illustrates the simulated frequency response for varied tap locations.

In Figure 5, the feedline tapping location is at 1 mm down referred to the brim of the square ring. However, when we vary the tapping location, a varied resonance is shown as in Figure 6.
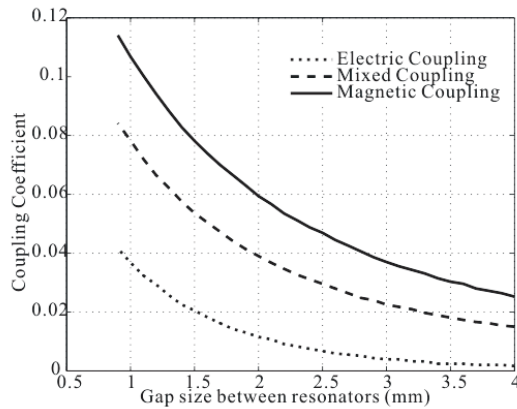

Figure 7. Extracted coupling coefficients versus gap size.

From Figure 6, it can be seen that as the tapping location rises up, the transmission peak around the resonant frequency goes up while its fractional bandwidth becomes slightly narrower. Thus, it causes the quality factor to be increased.

Using the procedure described in [7], the coupling coefficient can be extracted from the simulated results in Figure 4 under varied gap size. Figure 7 plots the extracted coupling coefficient as a function of gap size. Similarly, the external quality factor can be determined as a function of the tapping locations as discussed in [9].

Now, let's carry out the synthesis design of an actual bandpass filter on microstrip-line structure. For an example, a filter is designed with the specifications extracted from [9], i.e., central frequency (f_c), fractional bandwidth (FBW), three sets of pole/zero locations (T_{pole} and T_{zero}) and in-band return loss (RL).

$$f_c = 2.5\,\text{GHz}, \quad FBW = 6\%$$
$$T_{pole} = \pm 0.931, \pm 0.4; \quad T_{zero} = \pm 2.3 \quad RL = 46.05\,\text{dB} \tag{13}$$

Element values of the filter network in Figure 1 can be determined via Equation (10) under the specifications in (13).

$$g_1 = 0.949080, \; g_2 = 1.350854, \; J_1 = -0.117259, \; J_2 = 1.011884 \quad (14)$$

As all these element values are derived, their relevant coupling matrix can be obtained as below

$$M = \begin{bmatrix} 0 & 0.883170 & 0 & -0.123550 \\ 0.883170 & 0 & 0.749069 & 0 \\ 0 & 0.749069 & 0 & 0.883170 \\ -0.123550 & 0 & 0.883170 & 0 \end{bmatrix} \quad (15)$$

As expected, Equation (15) has similar calculated results as from [9]. The resultant matrix can be used to quantitatively describe the filtering performance of the network in Figure 1.

Figure 8 is the layout of a bandpass filter to be designed. Using the design curves in Figures 4 or 7 and Figure 6, all the dimensions of this filter, such as ring length, tap location and three unequal gap sizes, can be determined. The filter is designed on the RT/Duroid 6010 substrate with a thickness of 1.27 mm, permittivity of 10.8 and loss tangent of 0.0023. As the overall dimensions of this filter are decided, its performance is then simulated using Agilent ADS.
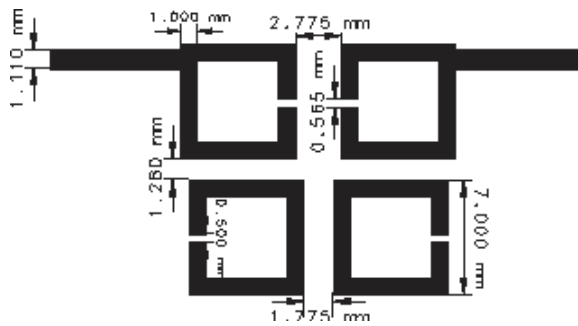

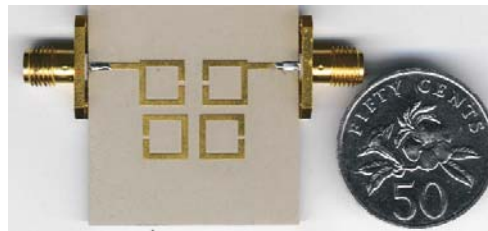**Figure 8.** Layout of the designed microstrip-line quadruplet filter.

Figure 9. Photo of the fabricated filter.

Figure 9 depicts the photograph of the fabricated microstrip-line quadruplet bandpass filter. Figure 10 is the comparison between the simulated and measured results. They are found in good agreement with each other over the frequency range of 2.2 to 2.7 GHz. The central frequency is about 2.45 GHz and the bandwidth is about 6.0% as can be observed from both simulated and measured results, thus reasonably achieving the specified ones as defined in Equation (13). Differed from the lossless network based synthesis design, the in-band insertion loss achieves 3.0 and 3.8 dB in simulation and experiment, respectively, due to unexpected conductor, substrate and radiation losses in practical implementation of narrowband filter.
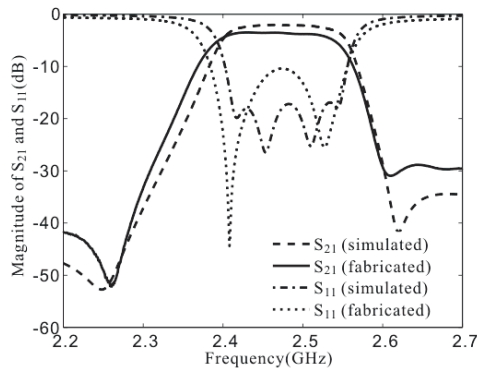

Figure 10. Simulated and measured results of the quadruplet filter.

5. CONCLUSION

This paper has presented an alternative synthesis methodology to numerically determine the element values of the folded quadruplet filter network. Its related two-port network parameters are defined and solved numerically according to the filter's specifications in priority. In order to annihilate redundancy in the over-determined coefficients, a determined solution is proposed and verified to carry out this design task with reasonably accurate element value table to the quadruplet structure. Furthermore, the determined coupling matrix is utilized to design a compact bandpass filter with the fractional bandwidth of about 6.0% centered around 2.4∼2.5 GHz. In final, a filter is physically fabricated for experimental validation of the presented methodology. With this verified methodology, different type of physical coupling structure such as in [11] and [12] could be attempted for implementing with advanced cross-coupled filter function.

REFERENCES

1. Atia, A. E. and A. E. Williams, "Narrow-bandpass waveguide filters," *IEEE Trans. Microw. Theory Tech.*, Vol. 20, No. 4, 258–265, Apr. 1972.

2. Atia, A. E., et al., "Narrow-band multiple-coupled cavity synthesis," *IEEE Transactions on Circuits and Systems*, Vol. 21, No. 5, 649–655, Sep. 1974.

3. Darlington, S., "Synthesis of reactance 4-poles which produce prescribed insertion loss characteristics," *J. Math. Phys.*, Vol. 30, No. 9, 257–353, Sep. 1939.

4. Cameron, R. J., "General coupling matrix synthesis methods for Chebyshev filtering functions," *IEEE Trans. Microw. Theory Tech.*, Vol. 47, No. 4, 433–442, Apr. 1999.

5. Cameron, R. J., "Advanced coupling matrix synthesis for microwave filters," *IEEE Trans. Microw. Theory Tech.,* Vol. 51, No. 1, 1–9, Jan. 2003.

6. Levy, R., "Filters with single transmission zeros at real or imaginary frequencies," *IEEE Trans. Microw. Theory Tech.*, Vol. 24, No. 4, 172–181, Apr. 1976.

7. Hong, J. S. and M. J. Lancaster, "Couplings of microstrip square open-loop resonators for cross-coupled planar microwave filters," *IEEE Trans. Microw. Theory Tech.*, Vol. 44, No. 12, 2099–2109, Dec. 1996.

8. Hong, J. S. and M. J. Lancaster, *Microstrip Filters for RF/Microwave Applications*, Wiley, New York, 2001.

9. Mongia, R. K., et al., *RF and Microwave Coupled-line Circuits*, Artech House, Norwood, 2007.

10. Pozar, D. M., *Microwave Engineering*, Wiley, Hoboken, 2005.

11. Saliminejad, R. and M. R. Ghafouri Fard, "A novel and accurate method for designing dielectric resonator filter," *Progress In Electromagnetics Research B*, Vol. 8, 293–306, 2008.

12. Bernardi, P., et al., "An equivalent circuit for EMI prediction in printed circuit boards featuring a straight-to-bent microstrip line coupling," *Progress In Electromagnetics Research B*, Vol. 5, 107–118, 2008.